Twophoton photodissociation dynamics of stateselected NO2

Laurence Bigio and Edward R. Grant

Citation: The Journal of Chemical Physics **87**, 360 (1987); doi: 10.1063/1.453581
View online: http://dx.doi.org/10.1063/1.453581
View Table of Contents: http://scitation.aip.org/content/aip/journal/jcp/87/1?ver=pdfcov
Published by the AIP Publishing

Two-photon photodissociation dynamics of state-selected NO_2

Laurence Bigio[a] and Edward R. Grant[b]
Department of Chemistry, Cornell University, Ithaca, New York 14853

(Received 23 June 1986; accepted 20 March 1987)

Quantum states of NO_2 are selected and then photodissociated by resonant two-photon photoexcitation. The total photolysis energy is scanned over a region from 50 cm^{-1} below to 300 cm^{-1} above the threshold for production of $NO(\tilde{X}\,^2\Pi) + O(^1D)$. This channel yielding excited oxygen is observed to dominate the production of vibrational ground state NO. Diatomic product J and Λ doublet state distributions are probed by resonant two-photon ionization. The photodissociation cross section for production of specific NO quantum states is found to be structured in the photolysis wavelength. This structure is assigned to intermediate resonance in the two-photon photolysis. Rotational structure is identified in this pattern, and confirmed by separate optical–UV–double resonance spectroscopy using the same intermediate states in combination with levels of the $3p\sigma\,^2\Sigma_u^+$ Rydberg state of NO_2. Though photodissociation dynamics are found to be a very sensitive function of photolysis wavelength, different wavelengths that promote different transitions through the same intermediate state yield very similar dynamics. The existence and apparent patterns of photoselection in the product state dynamics are discussed in the light of recent theoretical developments incorporating electronic degrees of freedom in state-to-state photofragmentation.

I. INTRODUCTION

Laser photodissociation in the ultraviolet is a well established and widely used technique for studying unimolecular fragmentation.[1–7] For experimental conditions under which nascent product state distributions can be determined free of collisional scrambling, photodissociation techniques can offer substantial insight concerning the dynamics of primary decomposition processes.

Theory, which ties observed final state distributions with the quantum evolution of a system driven from photoexcitation through dissociation, has made significant progress in the past few years.[8–18] It has now become possible to make definite predictions about final state distributions for given initial reactant quantum states for certain simple photodissociation systems. This raises new challenges for experiments. Theory demands a specified initial state, but in practice it is difficult to select an individual state from among many when photoexciting to a broadened band or continuum. The insertion of an intervening step of photoselection overcomes this limitation, and two new two-photon photodissociation techniques have been introduced in the past year.[7,17,19] Both yield important new levels of dynamical resolution.

One of these techniques is IR/UV double resonant photodissociation as developed for H_2O by Andresen and coworkers.[7,17] The other is optical–optical double resonant two-photon photodissociation developed in our laboratory for NO_2.[19] In our work, individual states of NO_2's bound optical absorption system are selected by the absorption of one visible photon. A second photon carries the system above the threshold for $NO_2 \rightarrow NO + O(^1D)$.

The channel to produce excited oxygen is observed to dominate the formation of vibrationally cold $NO(\tilde{X}\,^2\Pi, v = 0)$, which is detected by resonant two-photon ionization. For two-photon photolysis energies within 100 cm^{-1} of threshold, photodissociation dynamics, manifested in NO rotational and Λ doublet state distributions, are observed to depend sensitively on parent intermediate state. NO populations are an oscillatory function of product J, with varying patterns of Λ doublet preference that change with selected NO_2 intermediate state. The present work builds on our earlier preliminary study[19] by focusing on photodissociation at selected wavelengths for which intermediate states are angular momentum (N) labeled by separate optical–UV–double resonance (OUDR) spectroscopy.

Section II gives experimental details pertaining to techniques for two-photon photolysis and OUDR. Section III presents the main results of this work which consist of: (1) observations of the product state selected two-photon photodissociation cross section of NO_2 near the $O(^1D)$ threshold; (2) dynamics of NO production as a function of features selected in the photodissociation spectrum; (3) N labeling of relevant features by OUDR spectroscopy; and (4) estimation of the $O(^1D)/O(^3P)$ branching ratio. Section IV discusses the results and then establishes a qualitative connection between the present observations and a new theoretical approach developed by Balint-Kurti and co-workers to account specifically for electronic degrees of freedom in state-to-state photodissociation.[17] A paper to follow[20] will apply the results of polarization experiments to examine the question of rotational alignment of the NO product from two-photon photolysis.

[a] Present address: General Electric Research Center, P. O. Box 8, Bldg. K1-4C34, Schenectady, NY 12301.
[b] Address correspondence to this author at Department of Chemistry, Purdue University, West Lafayette, Indiana 47907.

 0021-9606/87/130360-10$02.10

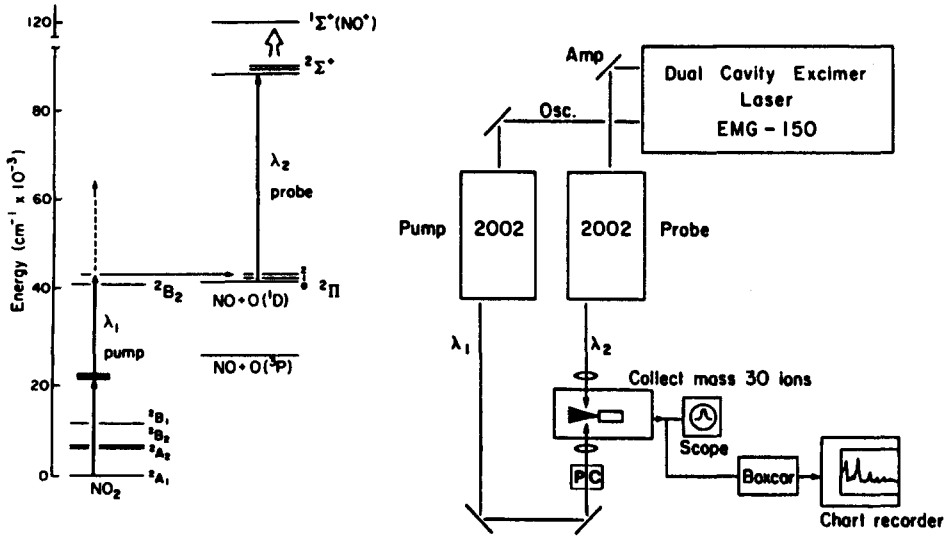

FIG. 1. (a) Energy diagram showing resonant 1 + 1 ionization of NO product following two-photon photodissociation of NO_2. (b) Experimental arrangement (PC = Pockels cell).

II. EXPERIMENTAL METHOD

A. Photodissociation

The experimental arrangement used for dissociation is similar to that described in an earlier paper.[19] A Lambda Physik EMG-150 ES excimer laser pumps two FL-2002 dye lasers which generate 12 ns laser pulses, each with 0.3 cm^{-1} bandwidth, separated temporally by 15 ns. These pulses are focused through a pair of 20 cm focal length lenses to counterpropagate across the output of an NRC BV-100 pulsed molecular beam valve. The foci overlap on the axis of the NO_2 jet (seeded 1:1:20 in O_2:Ar at 1 atm stagnation pressure) with the λ_1 pulse (pump) arriving first and the λ_2 (probe) second. A Pockels cell, placed in the pump beam path just before the molecular beam chamber, is used to rotate the polarization of the pump beam relative to the probe.

Nascent NO generated from the two-photon photolysis of the NO_2 by the pump beam is probed via standard 1 + 1 ionization spectroscopy by the probe beam. Mass-filtered ($m/e = 30$) NO ions are detected by a Galileo 4113 channeltron, the signal from which is amplified and then fed to a PAR 165/162 boxcar averager. Figure 1 gives an energy diagram showing the photodissociation and probe steps, as well as a schematic of the experimental setup.

Probe laser light in the region of 225 nm is generated by doubling Coumarim 450 (Exciton) in KB5. Second harmonic light is separated from the fundamental by an arrangement of four Brewster prisms. Energy per pulse at this point is typically 50 μJ or less. Variable attenuators reduce this further to a level the order of 1 μJ. At such intensities, the probe laser induced NO signal is observed to be accurately quadratic in the laser power, which we take to indicate that saturation effects are minimal.[21] Accordingly, we derive rotational populations by dividing measured intensities by $S_{J'J''}/(2J''+1)$, where the $S_{J'J''}$ are line strength factors.[22] Populations obtained using the P_{11} branch and the $(Q_{21}+R_{11})$ mixed branch, which both measure the same Λ doublet (Π^+), are compared and generally found to give equal population distributions, confirming for this Λ doublet that saturation effects, if present, are very small. For these two branches, results are averaged to establish the population distribution for the Π^+ Λ doublet. By contrast, the R_{21} and $(Q_{11}+P_{21})$ branches, which both measure the Π^- Λ doublet, occasionally show differences which can be attributed to saturation of the $(Q_{11}+P_{21})$ mixed branch. The latter has the largest Hönl–London factor of all four branches, while that for the R_{21} branch is the smallest. The $(Q_{11}+P_{21})$ branch also forms an inconvenient bandhead at low J. Therefore, Π^- Λ doublet populations are taken from the R_{21} branch only. Because its line strength factor is smaller than either P_{11} or $(Q_{21}+R_{11})$ branches, and because the latter two yield equal population distributions despite the difference in line strength factors between them, we conclude again that saturation effects do not significantly distort the reported populations of the two Λ doublets.

Finally, we take care to subtract a small background signal, seen with only the probe beam on, due to a trace amount of NO contaminant in the molecular beam. This background spectrum is useful for estimating the beam rotational temperature. We generally find that the lowest four J lines of the cold NO are thermalized at $\simeq 5$ K, with a small tail extending out to higher J.

B. Optical–UV–double resonance

Optical–UV–double resonance (OUDR) is used to confirm rotational quantum numbers assigned to the intermediate states involved in resonant two-photon photodissociation. Most of the experimental details are identical to those described above. The principal differences are that the counterpropagating laser beams are unfocused as they cross the molecular beam, and mass 46 ions, rather than mass 30, are

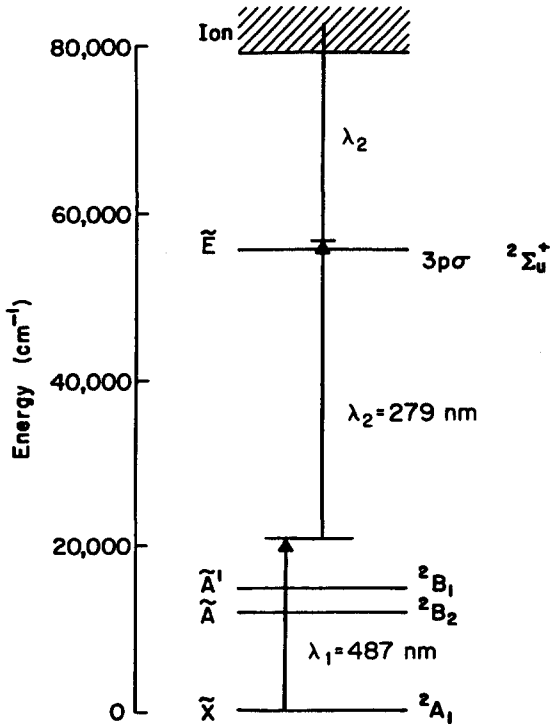

FIG. 2. Energy diagram for the OUDR experiment. Arrows are separated to indicate a delay of the λ_2 beam by ~ 10 ns from the λ_1 beam.

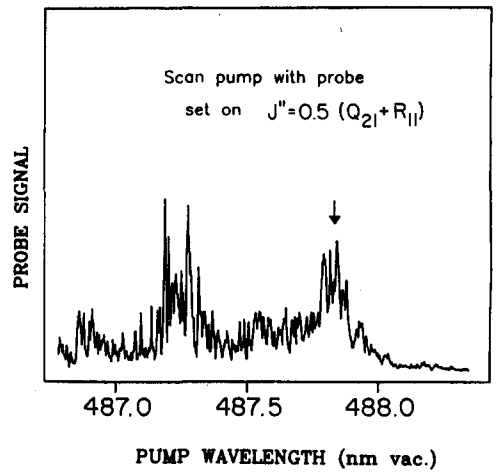

FIG. 3. Two-photon photolysis scan of the pump for the probe set on $(Q_{21}+R_{11})$ (0.5) [refer to Fig. 1(a)]. Arrow indicates $O(^1D)$ threshold.

collected. Also, for convenience the relative polarizations of the λ_1 and λ_2 beams are held perpendicular. The setup is thus nearly identical to Fig. 1(b). Figure 2 shows an energy diagram detailing the step-wise excitation.

In this experiment, two 12 ns pulse length laser beams again overlap spatially and are separated by 15 ns with the λ_1 beam arriving first. The λ_1 photon prepares a (nominally) stationary state in the 487 nm region. The λ_2 beam carries the excited NO_2 to ionization via resonance with either the (000) or (010) band of the $^2\Sigma_u^+$ Rydberg state in a $1+1$ process. Ionization signal is seen only when both steps are resonant, producing a signal/noise ratio of well over 100. Blocking either beam extinguishes signal. The fact that an unfocused λ_2 beam ionizes the NO_2 in a two-photon resonant process indicates that the cross section for ionization from the Rydberg state is high and that the Rydberg state is relatively stationary (an observation confirmed by measured rotational linewidths).

Either beam can be scanned while the other is fixed. The origin band of the $^2\Sigma_u^+$ state has been rotationally assigned by conventional two-photon absorption spectroscopy,[23] and the ground state is well characterized. From this information it is possible to assign double resonance spectra. Tuning the second beam (λ_2) with λ_1 fixed, is thus directly analogous to fixed (λ_1) frequency excitation with detection of the dispersed fluorescence. Tuning the first beam (λ_1) while keeping the second fixed is very nearly analogous to laser excited fluorescence, in which a single dispersed color is monitored while λ_1 is scanned.

This approach offers certain advantages over fluorescence for assigning rotational quantum numbers to intermediate states. Absolute signals are much stronger than dispersed fluorescence, and the bandwidth of λ_2 interrogation is that of a laser rather than a monochrometer. Total absorption undifferentiated by intermediate quantum state is also monitored by an EMI 9798B photomultiplier tube (not shown in Fig. 2) with a Schott OG 570 filter to block scattered laser light. The LIF spectrum, which in general is more congested than the OUDR spectrum, serves conveniently to set λ_1 on specific resonances.

C. Calibration of λ_1

Chromium lines are used to calibrate the λ_1 wavelength.[24] A simple ionization cell is filled with 0.1 Torr $Cr(CO)_6$ and 10 Torr CO. The λ_1 beam is focused through an 8 cm lens, and ions are collected by electrodes biased at 90 V. The current is amplified and sent to a boxcar averager as before. Following photolysis of the carbonyl, Cr is ionized in a $2+1$ process via the $a^5S_2 \rightarrow f^5D_{0,1,2,3}$ two-photon transitions. The λ_1 wavelengths reported here are corrected and listed as vacuum wavelengths.

III. RESULTS

A. Threshold for production of NO(v,J)

As noted previously[19] and discussed below, all product spectra of $NO(v''=0)$ show rotational population only up to an energy determined by the excess of the photolysis energy above the threshold for production of $O(^1D)$ (40 998 cm^{-1}).[4,25–27] This establishes that the photodissociation mechanism for production of NO ($v''=0$) must be

$$NO_2 \xrightarrow{2h\nu} NO(\tilde{X}\,^2\Pi, v''=0, J'', e/f) + O(^1D).$$

The apparent absence of a rotationally hot contribution to the $NO(v''=0)$ product distribution from the $O(^3P)$ channel is consistent with strongly inverted vibrational distributions observed to accompany $O(^3P)$ production at slightly lower energies by Slanger *et al.*[28]

Figure 3 shows a scan of λ_1 (pump) with λ_2 (probe) set on the $(Q_{21}+R_{11})$ (0.5) transition. Because the probe measures the population of the lowest J state of $NO(v'=0)$, a two-photon photolysis scan should give directly the thresh-

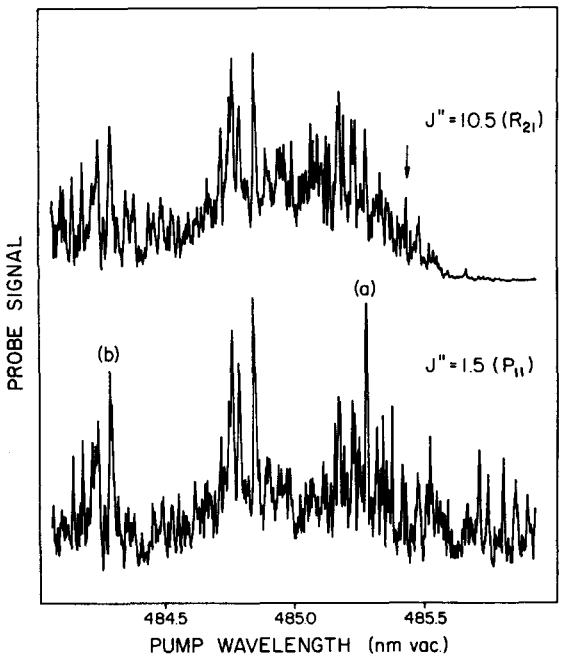

FIG. 4. Pump scans for probe set on $J = 10.5$ (R_{21}) (upper) and $J = 1.5$ (P_{11}) (lower). Arrow indicates threshold for creation of $NO(^2\Pi, v'' = 0, J'' = 10.5) + O(^1D)$ in the upper scan.

old for production of $O(^1D)$. This is seen in the figure by the onset of probe signal for $\lambda_1 < 488$ nm. With λ_1 calibrated in the manner discussed above, and with the $O(^1D)$ threshold known to be 40998 cm^{-1},[25] we place the absolute thermochemical threshold at the position on this spectrum marked by the arrow. The onset of signal starting below the arrow must be due to contributions from more energetic NO_2 initially in rotational states above the $N' = 0$ ground state. The energy spread from the true threshold (arrow) to 488 nm is about 15 cm^{-1}, thus indicating that the higher rotational states range to $N'' \simeq 6$, $K'' = 0$, or $N'' \simeq 3$, $K'' = 1$. This is consistent with estimates of the beam rotational temperature from this and previous work of $\simeq 20$ K.[19,29] Note that the polyatomic rotational temperature appears to be warmer than that implied by the spectrum of contaminant NO.

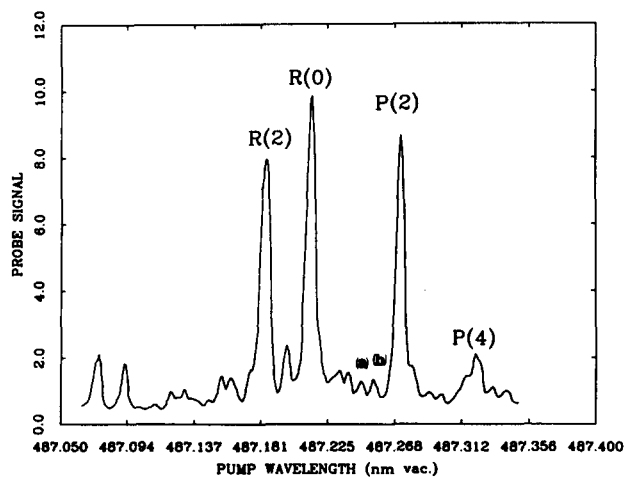

FIG. 5. Scan of the photolysis pump beam for the probe set on $J = 1.5$ ($Q_{21} + R_{11}$). Lines, indicating intermediate NO_2 state structure, are assigned and labeled accordingly (see the text).

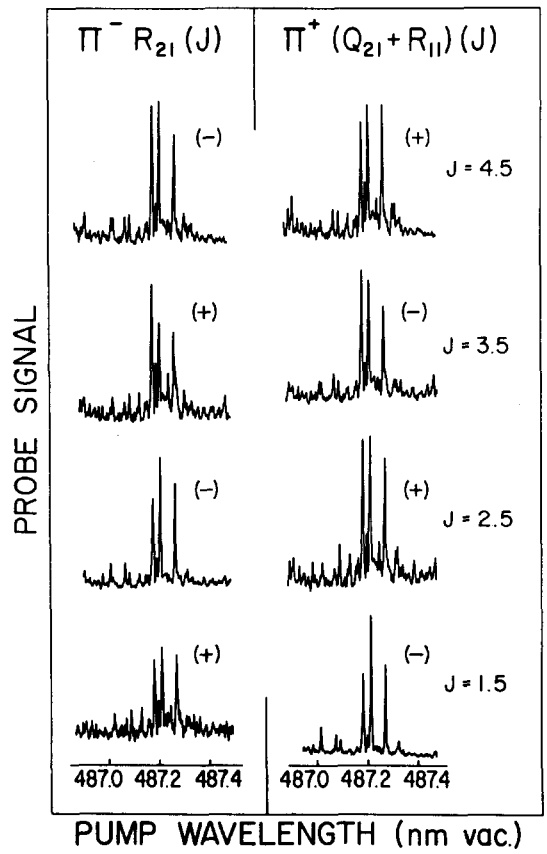

FIG. 6. Scans of the photolysis pump beam through same region as Fig. 5, for various product J and Λ doublet state transitions. Right column is for the probe beam set on Π^+ J states, and left column is for the probe set on Π^- J states. The total parity of the corresponding NO state is indicated next to each scan.

B. Structure in the photodissociation spectrum

The structure seen in Fig. 3 is easily reproducible. These scans give the two-photon absorption spectrum of NO_2 for photodissociation into a particular product quantum state, as specified by the probe transition. For example, we compare in Fig. 4, two bluer pump scans (485 nm region), for NO product $J'' = 1.5$ (lower) and 10.5 (upper). Once again the onset of probe signal in the upper trace marks the threshold for production of $NO(v'' = 0, J'' = 10.5)$ in the $O(^1D)$ channel (marked by the arrow). Though not obvious, a careful overlap of both traces shows an exact correspondence of all lines, with differences only in the relative intensities.

Figure 5 shows a similar scan of the pump wavelength with the probe set to the $(Q_{21} + R_{11})$ (1.5) transition. As previously noted,[19] the spacings of the main lines seen in this dissociation scan fit a spectral pattern recognized by Smalley, Wharton, and Levy to correspond to a parallel $\Delta K = 0$ $\tilde{X}\,^2A\,^1 \rightarrow \tilde{A}\,^2B_2$ transition.[30] This rotational assignment is confirmed by optical–UV–double resonance (see below).

These same features appear with varying absolute and relative intensities in scans for a range of product NO quantum states. Figure 6 shows scans for eight such final states ranging from $J = 1.5$ to 4.5 ordered by angular momentum and sorted by Λ doublet and total parity.

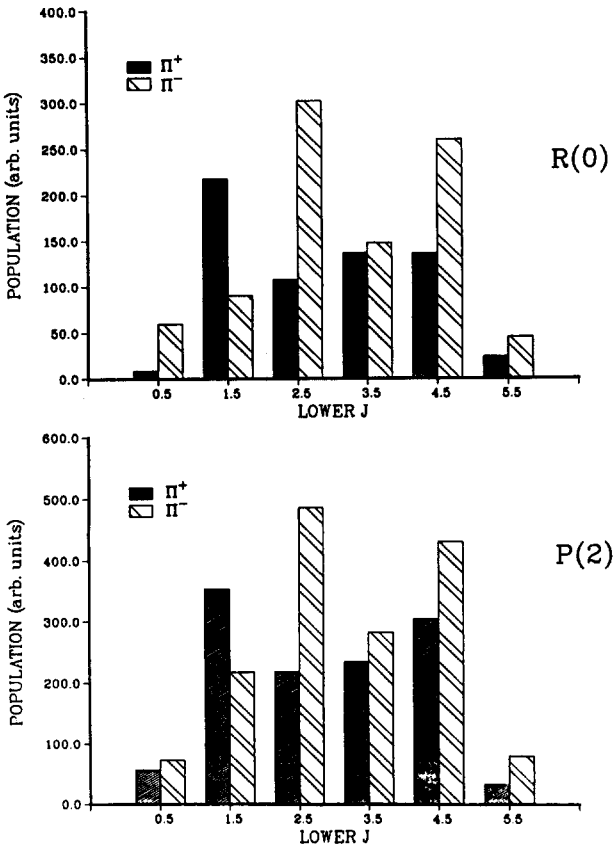

FIG. 7. Λ doublet rotational state population distributions of nascent NO for pump wavelengths set on the $R(0)$ (upper) and $P(2)$ (lower) peaks of Fig. 5. $R(0)$ and $P(2)$ both access the $N' = 1$ intermediate state of parent NO_2. Note the similar product Λ doublet distributions.

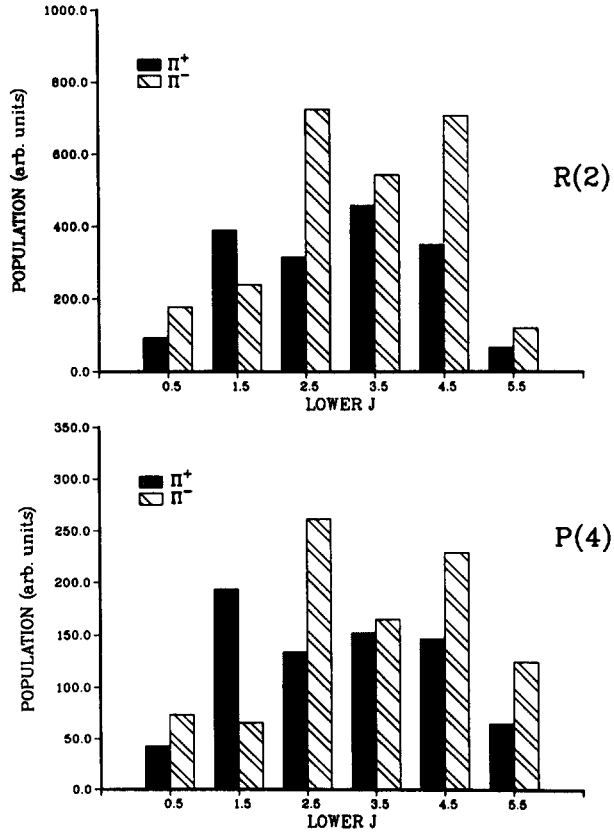

FIG. 8. Λ doublet distributions of nascent NO for pump wavelengths set on the $R(2)$ and $P(4)$ peaks of Fig. 5. $R(2)$ and $P(4)$ both access the $N' = 3$ intermediate state of parent NO_2. Note again similar product Λ doublet distributions.

C. Product state distributions following two-photon photolysis

Figures 7 and 8 compare the Λ doublet rotational state population distributions of product NO for pump wavelengths set on the $R(0)$ and $P(2)$ peaks (Fig. 7) and the $R(2)$ and $P(4)$ peaks (Fig. 8). These distributions are determined after first comparing parallel with perpendicular relative polarizations between the pump and probe beams. No differences are observed which exceed the $\sim 10\%$ experimental uncertainty. The distributions shown average at least four experimental scans each. Care is taken to monitor and properly normalize for probe laser intensity, though laser output is essentially flat over the short tuning range necessary to scan all of the relevant NO spectrum which extends only to about $J = 5.5$. Relative populations determined by weak transitions, such as $P(4)$, have a higher ($\sim 20\%$–30%) degree of experimental uncertainty than those from the stronger pump transitions, such as $R(0)$, $R(2)$, and $P(2)$ ($\sim 10\%$), due mainly to the contaminant NO background signal. However, on the whole, the different Λ doublet populations as well as their oscillatory patterns as a function of J (of the NO) are found to be quite reproducible.

Figures 9 and 10 show Λ doublet distributions for λ_1 set on the small peaks marked (a) and (b) in Fig. 5. Clearly the population distributions are different from each other as well as from those of Figs. 7 and 8. In fact, differences in the dynamics as a function of slight changes in the pump wavelength are the rule, while similarities such as those shown in Figs. 7 and 8 are exceptions.

We have also obtained the Λ doublet distributions for several higher photolysis energies between 200–300 cm^{-1} above the $O(^1D)$ threshold where we average the parallel and perpendicular polarization results (a specific discussion of alignment effects in these higher energy distributions is

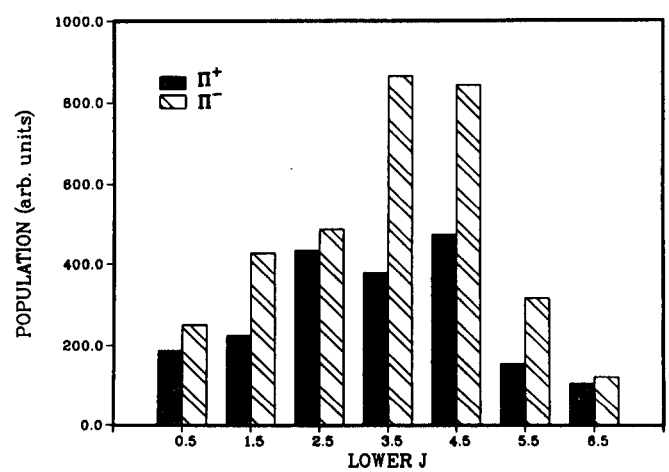

FIG. 9. Λ doublet distributions for pump wavelength set on peak (a) of Fig. 5.

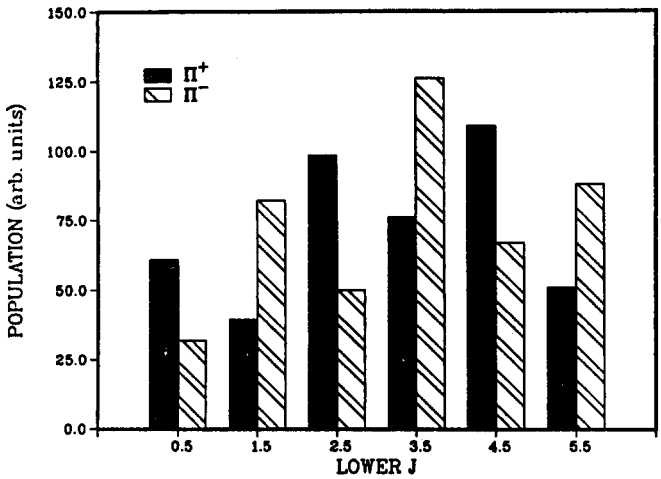

FIG. 10. Λ doublet distributions for pump wavelength set on peak (b) of Fig. 5.

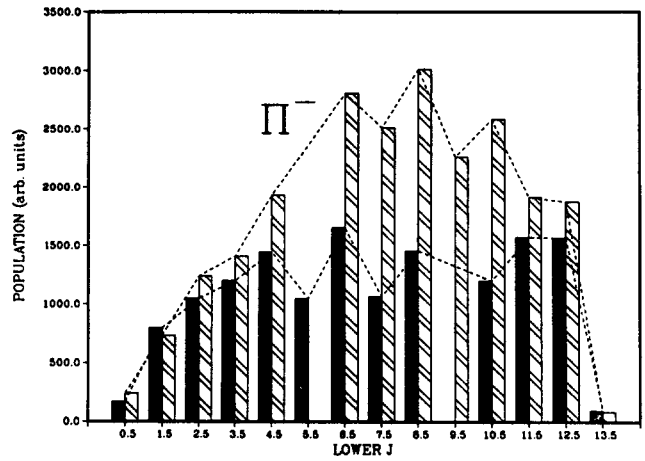

FIG. 12. Λ doublet populations for pump wavelength set on peak (b) of Fig. 4 at 299.2 cm^{-1} above the $O(^1D)$ threshold. Darker shading denotes Π^+ component; lighter denotes Π^- component.

reserved for a later paper[20]). Figures 11 and 12 show the NO rotational populations for λ_1 set on peaks (a) (215.1 cm^{-1}) and (b) (299.2 cm^{-1}) of the dissociation scan of Fig. 4. For these higher energies we find a general preference for the Π^- over the Π^+ Λ doublet.

D. Optical–UV–double resonance

A standard absorption spectrum of NO_2 at the level of the first photon shows a dense structure of sharp lines.[30,31] A second photon carries the system to a region about 1000 cm^{-1} above the origin of the 2^2B_2 state. This state is predissociated with a lifetime of 42 ps at the origin.[32] By the level of the $O(^1D)$ threshold, rotational structure is completely diffuse, and it is inferred that the lifetime falls to the subpicosecond regime.[23] We can thus expect any structure in such two-photon photodissociation scans as Figs. 3 through 6 that arises from the 2^2B_2 state at the level of the second photon to be tens of wavenumbers wide. The sharp structure seen in the present two-photon spectra must then be caused by intermediate states at the level of the first photon.

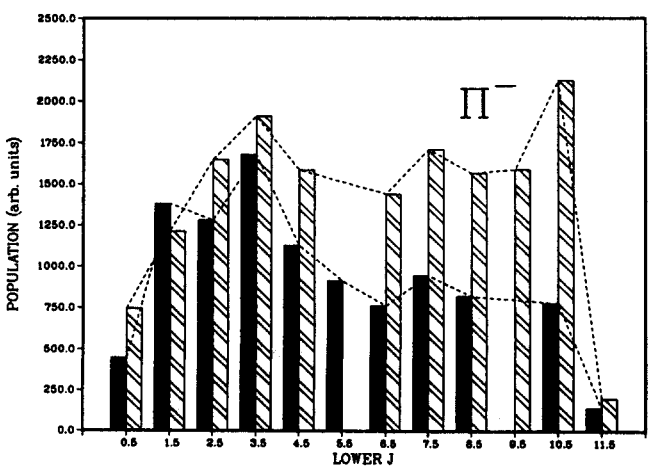

FIG. 11. Λ doublet populations for pump wavelength set on peak (a) of Fig. 4 at 215.1 cm^{-1} above the $O(^1D)$ threshold. Darker shading denotes the Π^+ Λ doublet; lighter denotes the Π^- component.

As mentioned above, elements of this structure can be assigned to states of total angular momentum N by analogy to spectra of Smalley, Wharton, and Levy.[30] These assignments are confirmed by optical–UV–double resonance (OUDR).

In OUDR, selected intermediate states are projected onto rotational manifolds of the ground (000) and lowest excited (010) vibrational levels of the $3p\sigma\ ^2\Sigma_u^+$ Rydberg state.[34] The (010) level is connected by the transformation properties of the Rydberg state together with those of the two-photon transition operator to levels $K'' = 0$ and 2 of the $^2A_1$ ground state. (000) is connected only to $K'' = 1$.[35]

A double resonance spectrum for λ_1 fixed on the transition labeled $R(2)$ in Fig. 5, and λ_2 scanned across the (010) Rydberg band is shown in Fig. 13. The characteristic PQR pattern from $N' = 3$ confirms the preliminary labeling of

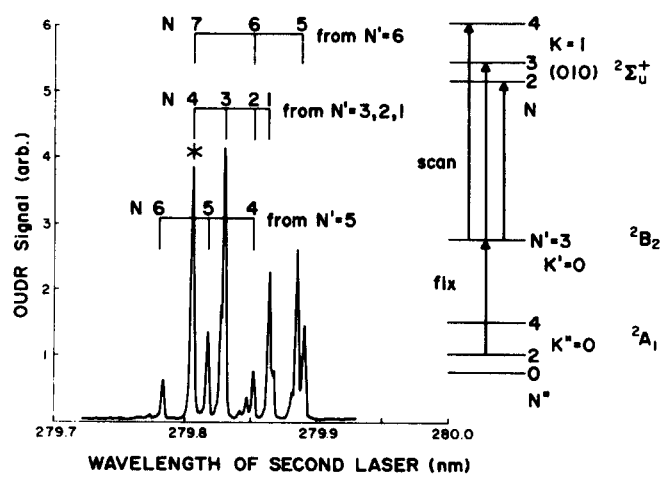

FIG. 13. OUDR scan of λ_2 to the (010) $^2\Sigma_u^+$ Rydberg state, with λ_1 set on the $R(2)$ peak of Fig. 5 [or Figs. 15(a) and 15(d)]. Diagram on right side shows λ_1 originating from the $K'' = 0$ stack, in this case from $N'' = 2$, and going to $K' = 0$, $N' = 3$ [thus the label $R(2)$ for λ_1]. Not shown in the diagram are other transitions that fall within the bandwidth of λ_1, similar to those shown in the diagram of Fig. 14, which add extra lines evident in the OUDR spectrum.

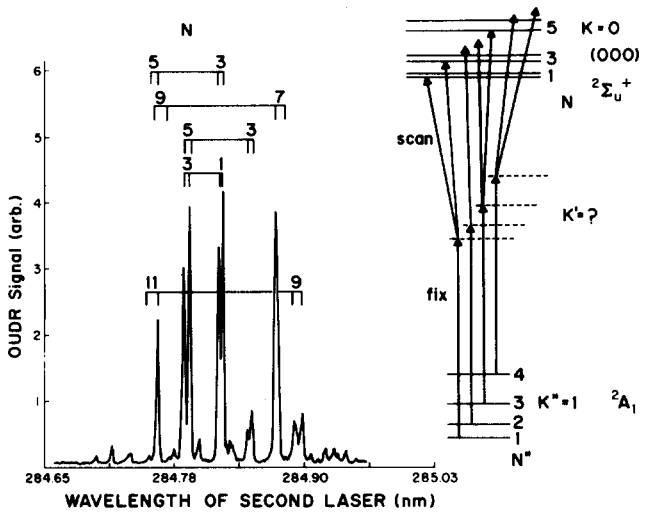

FIG. 14. OUDR scan of λ_2 to the (000) $^2\Sigma_u^+$ Rydberg state, with λ_1 set on the $R(2)$ peak of Fig. 5 [or Figs. 15(a) and 15(d)]. Diagram on right side illustrates added spectral complications due to the availability of several appropriate N' states in the densely spaced intermediate vibronic region. Splittings seen in the spectrum are due to spin–rotation splitting in the upper Rydberg state ($\tau = 0.13\ \text{cm}^{-1}$). All transitions observed in double resonance must originate from the $K'' = 1$ stack of the ground $^2A_1$ state, thus indicating a $K'' = 1$ contribution underlying the transition identified above as $^qR_0(2)$.

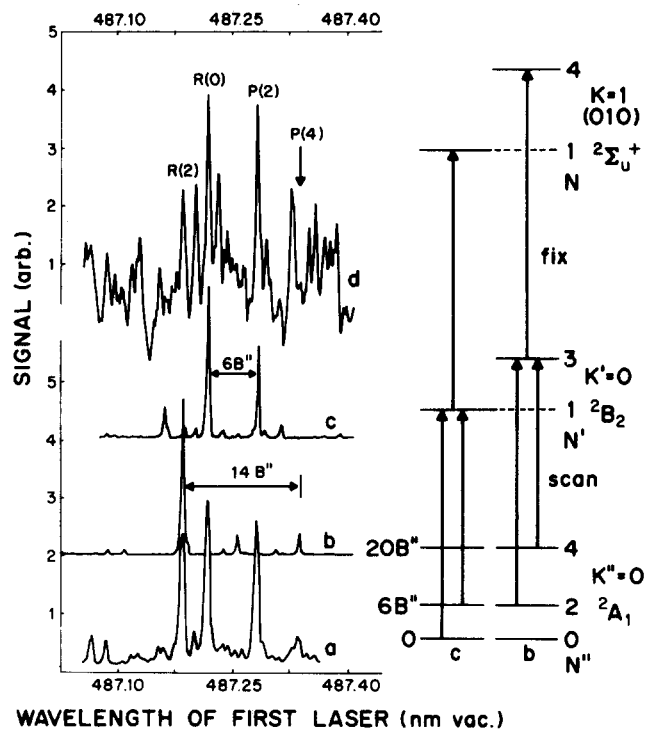

FIG. 15. (a) Dissociation scan of Fig. 5 drawn on the same scale as an LIF scan of the same region of NO_2, (d). Trace (b) is an OUDR scan of λ_1 with λ_2 fixed on the $N' = 3 \rightarrow N = 4$ transition, as shown in the corresponding diagram marked (b) on the right-hand side, and marked * in Fig. 13. Trace (c) is a similar OUDR scan of λ_1 with λ_2 set on the $N' = 1 \rightarrow N = 1$ transition, as shown in the corresponding diagram marked (c) on the right-hand side. Line separations in spectra (b) and (c) match ground state energy differences (see diagrams), and line positions in spectra (b) and (c) closely match line positions in spectra (a) and (d), thus confirming original assignment of the lines as denoted in trace (d) and Fig. 5.

this structure.[36] However, other bands evident in the spectrum show that additional intermediate states are also populated at this λ_1 wavelength. Indeed, the Rydberg level (000) shows a strong double resonance signal, as shown in Fig. 14, indicating that transitions originating from rotational states of the $K'' = 1$ sublevel are also active within this intermediate state band.

A determination of the total absorption cross section in this region can be obtained from the fluorescence excitation spectrum. This undifferentiated absorption spectrum as observed under our pulsed jet conditions is shown in Fig. 15(d), where it is compared with a resonant two-photon photodissociation spectrum over the same region [Fig. 15(a)].

These two absorption spectra of NO_2 are obviously very different. The total absorption spectrum is highly congested while the dissociation spectrum consists predominantly of the low-N four-line pattern mentioned above. In fact, the simpler spectrum of Fig. 15(a) is seen to be a subset of the more congested Fig. 15(d).

Verification of the assignment given the simple features of the photodissociation spectrum is directly achieved in double resonance by scanning λ_1 with λ_2 set on resonance for transitions between selected intermediate states and known rotational levels of the Rydberg state. The center traces of Fig. 15 show two such scans for second photon frequencies set on transitions from intermediate $N' = 1$ [as selected by first photon transitions $R(0)$ and $P(2)$] to Rydberg $N = 1$, and intermediate $N' = 3$ [as selected by first photon transitions $R(2)$ and $P(4)$] to Rydberg $N = 4$. The appearance of ground to intermediate resonances in λ_1 at wavelengths precisely matching the corresponding photodissociation features confirms the low-N assignments of these latter bands. Additional bands in these spectra represent accidental double resonances with other rotational levels of the Rydberg manifold, attesting again to the high density of available intermediate states.

E. $O(^1D)/O(^3P)$ branching ratio

Without yet a direct spectroscopic means to observe the $O(^1D)$ product, we attain a rough estimate of the $O(^1D)/O(^3P)$ branching ratio by comparing parts of the spectrum of NO that we know arise from dissociation via the $O(^1D)$ channel with parts that arise from dissociation via the $O(^3P)$ channel. Setting the pump beam (λ_1) on the $R(0)$ transition, at a two-photon photolysis energy of $51.53\ \text{cm}^{-1}$ above the $O(^1D)$ threshold, we scan the probe through the $\tilde{X}(^2\Pi_{1/2}, v'' = 0) \rightarrow \tilde{A}(^2\Sigma, v' = 0)$ transition in the 226 nm region, and the $\tilde{X}(^2\Pi, v'' = 6) \rightarrow \tilde{C}(^2\Pi, v'' = 1)$ transition in the 227.7 nm region. We find that a typical rotational line in the $\tilde{X} \rightarrow \tilde{A}$ transition, which has a Franck–Condon factor of 0.17, is about 25 times more intense than a typical line in the $\tilde{X} \rightarrow \tilde{C}$ transition, which has a Franck–Condon factor of 0.1.[37] We have already shown that, at this photolysis energy, spectra for $v'' = 0$ NO are due to dissociation via the $O(^1D)$ channel only, while $v'' = 6$ spectra can come only from the $O(^3P)$ channel. A measure of the branching ratio is given by

the total amount of NO produced in $v'' = 0$ vs the amount of vibrationally excited NO. Slanger *et al.* report that at about 800 cm^{-1} lower in photolysis energy, NO product is produced via the $O(^3P)$ channel, with essentially all the vibrational distribution concentrated in $v'' = 6$, 7 and 8 and at a ratio of roughly 1:2.5:2.[28] Thus, having measured the intensity of a typical rotational line of $v'' = 6$, we assume a democratic distribution over 50 rotational states weighted by 1, together with a similar distribution for $v'' = 7$ weighted by 2.5, and one for $v'' = 8$ weighted by 2. This, divided by the Franck–Condon factor for the $\tilde{X}\, v'' = 6 \rightarrow \tilde{C}\, v' = 1$ transition, will approximate the relative weight of the $O(^3P)$ channel. For the $O(^1D)$ channel we take the Franck–Condon corrected intensity of a rotational line for $v'' = 0$ and assume a democratic distribution over five rotational states. We conclude from this procedure that the overall $O(^1D):O(^3P)$ branching ratio is approximately 1:4.

IV. DISCUSSION

A. State-selected dynamics

The results presented above show that both product state distributions and detailed photodissociation cross sections in the two-photon photodissociation of NO_2 vary sharply with photodissociation wavelength. Structure in the photodissociation spectrum can be clearly associated with specific low-N intermediate states that present large absorption cross sections for photoproduction of specific low-N final states. In particular, such spectra show prominent $P(2)$ and $R(0)$ transitions to a common intermediate of $N' = 1$, and $P(4)$ and $R(2)$ transitions to $N' = 3$. Though photodissociation in each case proceeds through the same intermediate state, final energies in the 2^2B_2 continuum are slightly different. Yet, with subpicosecond final state lifetimes, coupling widths are tens of wave numbers wide. Thus, it is interesting to ask whether state selectivity at the intermediate level persists to affect the dynamics of final quantum state distribution in the products.

Returning to experimental results, distributions for intermediate states now labeled as $N' = 1$ via transitions identified as $P(2)$ and $R(0)$ are shown in Fig. 7 and for $N' = 3$ via $P(4)$ and $R(2)$ in Fig. 8. The degree of similarity within these sets is striking. By contrast, distributions for photolysis wavelengths slightly off-resonant with respect to identified low-N transitions differ strongly. The data presented in Figs. 9 and 10 are typical.

At this point it is interesting to recall the comparison between the photodissociation spectrum and that for total absorption as presented in Fig. 15, as well as the complexity evident in the multiple N' character of the double resonance spectra. It is clear that photoexcitation, even on a low-N intermediate resonance, prepares many higher-N intermediate states as well, yet the dissociation dynamics is dominated by that particular low-N component of the multiple resonance. This selectivity simply reflects the fact that photodissociation cross sections for production of the cold NO products accessible near threshold are evidently much larger for low-N NO_2 parents, and, when these species are photoselected, their contributions dominate the observed dynamics. The cross section for production of rotationally cold NO from hot NO_2 is finite, however, and of the order of the continuous background underlying the strong low-N resonances in Figs. 5–7. Furthermore, the behavior at threshold shows that parent rotational energy can be used to overcome potential energy and produce low internal angular momentum products.

Also interesting are the similarities between the $N' = 1$ and $N' = 3$ distributions. We suggest below that this result may reflect the fact that the photopreparation in both cases proceeds through odd-numbered low-angular momentum intermediate states. These states have negative total parity. Examining closely the complementary information in the collected photodissociation spectra of Fig. 6, we observe in all cases the distinctive $R(2)$, $R(0)$, $P(2)$, and $P(4)$ pattern discussed above. Their prominence relative to the background of states, however, appears greatest when the probe laser frequency is fixed on transitions of NO product states of negative total parity.[38] This propensity to conserve parity is confirmed for all accessible product states by careful examination of Figs. 7 and 8 (see Fig. 4 of Ref. 19 for parity ordering of NO rotational states).

At higher photolysis energy, away from apparent low-N intermediate resonances, this propensity shifts to one of uniform Π^- electronic symmetry over Π^+. Unfortunately, unlike photodissociation studies of H_2O in which the $OH(^2\Pi)$ dissociation partner is the spherically symmetric $H(^2S)$ atom,[5,39] we cannot here use Λ doublet preference results for NO to predict the electronic symmetry of the photoprepared NO_2 parent, because we do not know the symmetry of the $O(^1D)$ partner, and we have yet to find a convenient transition for measuring the $O(^1D)$ M_L levels (quantized by the O–NO axis[40,41]).

B. Product state dynamics in a state-selected Franck-Condon limit

Recent theoretical work by Balint-Kurti and coworkers predicts Λ doublet population distributions for $OH(^2\Pi)$ following one-photon photodissociation of H_2O ($\tilde{X}\,^1A_1$) via the $\tilde{A}\,^1B_1$ state.[17] The relative population of the j rotational state of the diatom, with Λ doublet and spin–orbit component specified by l, is given by

$$P_{jl} \sim \sum_{Jk\lambda} (2J+1)(2k+1) t_\lambda^2 \times \left| \sum_{j''\lambda''} C_{j''\lambda''}^{J_i P_i} \cdot t_{\lambda''} \cdot \{ [J - \lambda \,|J_i \lambda''](-1)^\lambda + P_i (-1)^{J+J_i} [J\lambda \,|J_i \lambda'']\} F_l(jk\lambda \,|j''\lambda'') \right|^2 .$$

The $C_{j''\lambda''}^{J_i P_i}$ factors are expansion coefficients of the triatomic ground state radial wave function in terms of parity adapted angular basis functions. We will not define all the other symbols, which include rotation matrices, Clebsch–Gordan coefficients, etc., as these are given in Ref. 17. However, we will note the presence of a phase factor $(\pm)(-1)^{k-j+1/2}$ inside the term $F_l(jk\lambda \,|j''\lambda'')$ which, along with the $C_{j''\lambda''}^{J_i P_i}$ coefficients, cause Λ doublet distributions to oscillate as a function of j, with the Π^+ and Π^- components out of phase. The

presence of such a term is in qualitative agreement with the results presented here, and is equivalent to the interpretation given in our earlier paper of a propensity for production of final NO states of prefered total parity,[19] since the parity alternates with j oppositely for the two Λ doublets (see Fig. 4 of Ref. 19).

We also note another phase factor $P_i(-1)^{J+J_i}$ which we believe is partially responsible for the similarity in the dynamical results between Figs. 6 and 7. The total parity of the initial triatomic state (analogous, in our case, to the intermediate state in the two-photon excitation) is given by $P_i(-1)^{J_i}$. The final triatomic state has angular momentum J, which satisfies the triangle condition with J_i and 1. For two different values of J_i being compared, the phase factor $P_i(-1)^{J+J_i}$ will be the same for the various possible J values respectively, *if* the two J_i numbers are both even or both odd and belong to the same electronic state. In our case of doublet NO_2, J and J_i are replaced by N and N_i, where we have labeled N_i as N'. Thus, one might expect that the dynamical results for $N'=1$ ($^2B_2$) would look similar to those for $N'=3$ ($^2B_2$) since both intermediate states are odd and close in value. That they are close in value means that the other factors in Eq. (1) (Clebsch–Gordan coefficients, etc.) would also be close in value. This is evidenced experimentally by the similarity between Figs. 6 and 7.

To attempt a quantitative comparison of the present experimental results with theory, as has been done with good success for H_2O,[17] the development of Eq. (1) would have to be adapted for the more complicated case of NO_2 dissociation. The NO dissociation partner can be either $O(^1D)$ or $O(^3P)$, which are both energetically allowed, while the intermediate state, which may be considered as the initial state in a one-photon excitation, is a vibronic mix of several electronic states. Furthermore, final state-interactions, which are justifiably ignored for the case of H_2O, could be significant here. While partial adaptations of the theory may be straightforward, a full calculation would at present be difficult.

V. SUMMARY

Two-photon dissociation of NO_2 at wavelengths below 488 nm yields $O(^1D)$ and $NO(X\,^2\Pi, v=0)$ in rotational states of energy up to but not exceeding the maximum permitted by the thermochemical threshold for this higher energy channel. A contribution from the $O(^3P)$ channel is found distributed over many rotational states of vibrationally excited NO. The wavelength dependent photodissociation cross section for production of specified $NO(v''=0)$ product rotational states is highly structured in the first photon wavelength. However, this photodissociation spectrum is simpler than the total absorption spectrum. This simplification arises from a suppression of higher-N lines in the photodissociation spectrum; the cross section for production of NO in the low-N final states accessible near threshold is evidently much higher for low-N parent NO_2.

On and off low-N intermediate resonance, we find Π^+ and Π^- Λ doublet distributions that differ from each other in a somewhat oscillatory pattern of opposite phase in product J. Fragmentation dynamics are a very sensitive function of photolysis wavelength. Even slightly different pump wavelengths yield different overall distributions. However, pairs of photolysis wavelengths that, through different transitions, access the same intermediate state, yield very similar final rotational state and Λ doublet distributions. Similar dissociation dynamics are seen as well for pump wavelengths that access two different intermediate states, both of which, though, are odd numbered low angular momentum states ($N''=1$ and 3).

For several energies farther above threshold (>200 cm^{-1}) we find an apparent propensity for generation of the Π^- Λ doublet over Π^+. This information, however, is not sufficient to deduce the electronic symmetry of the final parent state because no information is available on the symmetry of the $O(^1D)$ dissociation partner.

We note the qualitative agreement of the above Λ doublet distribution results with theory developed by Balint-Kurti and co-workers,[17,18] and with results from similar experimental photodissociation experiments on H_2O done by Andresen and coworkers.[7,17] Out-of-phase oscillatory Λ doublet populations are predicted by the theory for one-photon photodissociation from a well defined initial angular momentum state. We have seen that the two-step double resonance photodissociation conducted here can be regarded approximately as a one-photon photodissociation from specific intermediate angular momentum state. Thus it seems reasonable to propose that an appropriate adaptation of the theory (developed for H_2O) could successfully account for the photodissociation dynamics of state-selected NO_2.

ACKNOWLEDGMENTS

This work was supported by the U. S. Army Research Office. Acknowledgment is gratefully made to the Department of Defense for a DOD–University Research Instrumentation Grant.

[1] J. P. Simons, J. Phys. Chem. **88**, 1287 (1984).
[2] R. Bersohn, J. Phys. Chem. **88**, 5195 (1984).
[3] S. R. Leone, Adv. Chem. Phys. **50**, 255 (1982).
[4] A. Hodgson, J. P. Simons, M. N. R. Ashfold, J. M. Bayley, and R. N. Dixon, Mol. Phys. **54**, 351 (1985).
[5] R. Vasudev, R. N. Zare, and R. N. Dixon, J. Chem. Phys. **80**, 4863 (1984).
[6] K. H. Welge, NATO ASI Series, Ser. B **105**, 123 (1984).
[7] P. Andresen, G. S. Ondrey, B. Titze, and E. W. Rothe, J. Chem. Phys. **80**, 2548 (1984); P. Andresen, V. Bershausen, D. Hausler, H. W. Luff, and E. W. Rothe, J. Chem. Phys. **83**, 1429 (1985).
[8] K. F. Freed and Y. B. Band, in *Excited States*, edited by E. C. Lim (Academic, New York, 1977), Vol. 3, p. 109; Y. B. Band and K. F. Freed, J. Chem. Phys. **63**, 3382 (1975); **67**, 1462 (1977); **68**, 1292 (1978); M. D. Morse, K. F. Freed, and Y. B. Band, *ibid.* **70**, 3604, 3620 (1979); M. D. Morse and K. F. Freed, *ibid.* **74**, 4395 (1981); **78**, 6045 (1983).
[9] W. H. Gelbart, Annu. Rev. Phys. Chem. **28**, 323 (1977).
[10] E. J. Heller, J. Chem. Phys. **68**, 2066, 3891 (1978).
[11] M. S. Child and H. Shapiro, Mol. Phys. **48**, 111 (1983).
[12] M. Shapiro and R. Bersohn, Annu. Rev. Phys. Chem. **33**, 409(1982).
[13] G. G. Balint-Kurti and M. Shapiro, Chem. Phys. **61**, 137 (1981).
[14] R. W. Heather and J. C. Light, J. Chem. Phys. **78**, 5513 (1983).
[15] R. N. Dixon, Mol. Phys. **54**, 333 (1985).
[16] R. Schinke, V. Engel, and V. Staemmler, Chem. Phys. Lett. **116**, 165 (1985).
[17] R. Schinke, V. Engel, P. Andresen, D. Hausler, and G. G. Balint-Kurti,

Phys. Rev. Lett. **55**, 1180 (1985); G. G. Balint-Kurti, J. Chem. Phys. **84**, 4443 (1986).
[18]R. Schinke, J. Phys. Chem. **90**, 1742 (1986).
[19]L. Bigio and E. R. Grant, J. Phys. Chem. **89**, 5855 (1985).
[20]L. Bigio and E. R. Grant (to be published).
[21]In a recent paper, Zare and co-workers demonstrate that partial saturation effects appear in the $\tilde{X}\,^2\Pi \rightarrow \tilde{A}\,\Sigma^+$ absorption spectrum in the lowest range of laser intensities typically used to promote resonant two-photon ionization. Such effects, combined with those of intermediate alignment on the cross section for the ionization step, can cloud the extraction of population and alignment information from resonant two-photon ionization spectra. By strongly attenuating our probe laser and working over a narrow range of product rotational quantum numbers, we believe our application of conventional signal averaging methods, combined with standard line strength corrections, yields population estimates that are accurate to within the stated uncertainties. More universally though, the Zare method of pulse-to-pulse energy normalization using the appropriate rate equations is to be preferred. See, D. C. Jacobs and R. N. Zare, J. Chem. Phys. **85**, 5457 (1986); D. C. Jacobs, R. J. Madix, and R. N. Zare, *ibid.* **85**, 5469 (1986).
[22]L. T. Earls, Phys. Rev. **48**, 423 (1935); see also Refs. 18–22 of Ref. 20.
[23]M. B. Knickelbein, K. S. Haber, L. Bigio, and E. R. Grant, Chem. Phys. Lett. **131**, 51 (1986).
[24]C. E. Moore, Natl. Stand. Ref. Data Ser. Nat. Bur. Stand. 35 (1971), Vol. II, p. 1.
[25]References 6 and 26 measure the $O(^3P)$ threshold to be 29 130 cm^{-1}. Adding the excitation energy of $O(^1D)$ (Ref. 26), places the threshold for photoproduction of $O(^1D)$ at 40 998 cm^{-1}.
[26]C. H. Chen, D. W. Clark, M. G. Payne, and S. D. Cramer, Opt. Commun. **32**, 391 (1980).
[27]C. E. Moore, Natl. Stand. Ref. Data Ser., Natl. Bur. Stand. 3, Sec. 7, A8 I-2 (1976).
[28]T. G. Slanger, W. K. Bischel, and M. J. Dyer, J. Chem. Phys. **79**, 2231 (1983).
[29]L. Bigio and E. R. Grant, J. Chem. Phys. **83**, 5361 (1985); R. S. Tapper, R. L. Whetten, G. S. Ezra, and E. R. Grant, J. Phys. Chem. **88**, 1273 (1984).
[30]R. E. Smalley, L. Wharton, and D. Levy, J. Chem. Phys. **63**, 4977 (1975).
[31]E. Haller, H. Koppel, and L. S. Cederbaum, J. Mol. Spectrosc. **111**, 377 (1985); Chem. Phys. Lett. **101**, 215 (1983).
[32]K.-E. J. Hallin and A. J. Merer, Can. J. Phys. **54**, 1157 (1976).
[33]W. M. Uselman and E. K. C. Lee, Chem. Phys. Lett. **30**, 212 (1975). See also G. Herzberg, *Electronic Spectra of Polyatomic Molecules* (Van Nostrand–Reinhold, New York, 1966), pp. 482–3.
[34]The fact that these intermediate states have Franck–Condon overlap with both the bent ground state and the linear Rydberg state reflects the highly mixed vibronic nature of these states. A more detailed discussion of this and the use of OUDR to expand these mixed states in the Rydberg zero-order bands is forthcoming.
[35]We ignore transitions from $K'' > 1$ as these have populations less than 10% of $K'' = 0$. See Ref. 29.
[36]In addition to $N' = 3$, there must be another state(s), either $N' = 2$ or 1 (or both), which is nearly degenerate with the $N' = 3$ state to account for the excitation of $N = 1$ in the final state, along with 2, 3, and 4.
[37]For a table of NO Franck–Condon factors, see Aerospace Report No. TR-0074 (4641)-6, Vol. II, p. N-35 (1974).
[38]In our earlier paper (Ref. 19) we assigned this $P = (-)$ propensity only to the $R(0)$ line [marked (C) in that work]. However, we now believe that the effect was simply accentuated in that case by a lower overall $R(0)$ intensity which pulled its signal into the background for $P = (+)$ scans. Such a lower intensity might have been caused by warmer beam conditions at the time.
[39]P. Andresen and E. W. Rothe, J. Chem. Phys. **82**, 3634 (1985).
[40]R. J. Van Brunt and R. N. Zare, J. Chem. Phys. **48**, 4304 (1968).
[41]M. H. Alexander and P. J. Dagdigian, J. Chem. Phys. **80**, 4325 (1984).